GEOLOGICAL JOURNAL
Geol. J. (2013)
Published online in Wiley Online Library
(wileyonlinelibrary.com). DOI: 10.1002/gj.2501

Large earthquake-triggered liquefaction mounds and a carbonate sand volcano in the Mesoproterozoic Wumishan Formation, Beijing, North China

DECHEN SU[1,2], XIUFU QIAO[1], AIPING SUN[1,2], HAIBING LI[1,2] and IAN D. SOMERVILLE[3]

[1] *Institute of Geology, Chinese Academy of Geological Sciences, Beijing 100037, China*
[2] *State Key Laboratory of Continental Tectonics and Dynamics, Beijing 100037, China*
[3] *School of Geological Sciences, University College Dublin, Belfield, Dublin 4, Ireland*

Ten well-preserved, earthquake-triggered liquefaction mounds and a carbonate sand volcano have been found in the Mesoproterozoic Wumishan Formation (1550–1400 Ma) in the Beijing area, North China. These features crop out in a roadcut near Zhuanghuwa Village. All ten mounds occur in the same sedimentary layer and have rounded shapes with some concentric and radial fissures arising from the centre. They range from 1.5 to 4 m in diameter and from 10 cm to 30 cm in height. The carbonate sand volcano has a diameter of 110 cm and the 'crater' at the top has a depth of about 30 cm. Associated with these mounds and the sand volcano are many 'normal' sedimentary structures and numerous soft-sediment deformation structures. The former include ripple marks, cross-bedding, stromatolites and desiccation cracks, indicating deposition in a stable shallow-water peritidal platform environment. The latter include intrastratal faults and folds, seismically formed breccias and carbonate clastic dykes. The morphological features and the genesis of these liquefaction mounds are very similar to mounds formed recently by the great Wenchuan Earthquake of China (2008). Detailed thin-section study of the mounds found no signs of any kind of biological constructional process; instead it reveals some obvious fluidification and liquefaction characteristics. Comparative studies have shown that these features are probably the products of Mesoproterozoic earthquake activity. Copyright © 2013 John Wiley & Sons, Ltd.

Received 21 November 2012; accepted 13 February 2013

KEY WORDS liquefaction mound; carbonate sand volcano; clastic dyke; Wumishan Formation; Wenchuan Earthquake; Mesoproterozoic; China

1. INTRODUCTION

Sediment liquefaction is the transformation of granular material from a solid state into a liquefied state as a consequence of increased pore-water pressures (Youd, 1973). Unconsolidated and water-saturated sediments can be easily liquefied by strong earthquake vibrations, forming liquefaction-induced dykes, vented sand sills, mounds, and sand volcanoes. Earthquake-triggered liquefaction hazards have been severe and widespread in modern-day areas affected by strong earthquakes (Takahama *et al*., 2000). Thus, these features have been extensively studied and used for palaeoseismic analysis, particularly in the disciplines of engineering and soil mechanics, to estimate the recurrence interval and magnitude of strong earthquakes (Obermeier, 1996, 1998).

However, most of these features, especially the liquefaction mounds and sand volcanoes, are normally exposed to erosion and/or abrasion by bottom currents and/or waves, and are rarely preserved in the geological record (van Loon and Maulik, 2011). Some of the earliest documented occurrences of sand volcanoes are from the Upper Carboniferous in western Ireland (Gill and Kuenen, 1958) and from the Early Permian in eastern India, and liquefaction-induced mounds have only been identified in Holocene sediments (Obermeier, 1996, 1998; van Loon and Maulik, 2011).

Most earthquake-triggered, soft-sediment deformation structures (SSDS) have been frequently reported in clastic sediments (sands, clays, silts and mudstones) (Owen, 1987, 1996; Obermeier, 1996, 1998; Rossetti and Góes, 2000; van Loon, 2009; van Loon and Maulik, 2011). Carbonates and evaporites, however, have been generally ignored in most attempts to understand earthquake-triggered, soft-sediment deformation (but see Bachmann and Aref, 2005; Ettensohn *et al*., 2011). Bachmann and Aref (2005) summarized three reasons for the scarcity of reports of earthquake-triggered SSDS in evaporites (which are similar to those for carbonates): (1) the cohesive behaviour of dolomite and gypsum and the possible low-susceptibility to liquefaction;

* Correspondence to: S. Dechen, Institute of Geology, Chinese Academy of Geological Sciences, Beijing, 100037, China.
E-mail: sudechen@gmail.com

(2) diagenetic processes that obliterate former depositional and early diagenetic structures; and (3) the apparent similarity of crystallization structures with deformational structures produced by seismic shock and shaking or other triggering mechanisms. The speed of cementation in carbonate sediments is much higher than that for most clastic sediments, and as a consequence it is really difficult to form large liquefaction features when an earthquake happens. These reasons could similarly be used to explain the scarcity of reports of earthquake-triggered SSDS in carbonates.

However, earthquake-triggered SSDS have been widely distributed and preserved in carbonate rocks, especially in the well-laminated and thinly-bedded carbonate layers, such as in the Wumishan Formation in North China. We have identified a number of well-preserved carbonate liquefaction mounds and one carbonate sand volcano in the Mesoproterozoic Wumishan Formation (1550–1450 Ma) along a roadcut section about 100 m long near Zhuanghuwa Village, *ca*. 70 km west of Beijing. We also have found numerous other SSDS in carbonates, such as clastic dykes, fragmented breccias, and syndepositional faults and folds near this section.

The aims of this manuscript are: (1) to report the discovery of liquefaction mounds and a carbonate sand volcano in the Mesoproterozoic Wumishan Formation (epicontinental carbonates); (2) to describe the carbonate liquefaction mounds, the sand volcano and other associated SSDS; and (3) to discuss the potential triggering mechanisms of these features by comparing them to similar features induced by the recent Wenchuan Earthquake (Ms 8.0) in Sichuan Province, SW China in 2008.

These liquefaction mounds and the associated SSDS represent some of the largest earthquake-triggered products documented from Proterozoic carbonates.

2. GEOLOGICAL SETTING

Located in the northern part of the Sino-Korean Palaeo-Plate (North China Craton), the Yan-Liao Aulacogen is a vast area that received voluminous sediments during the Meso- and Neoproterozoic eons (Fig. 1; He *et al*., 2000; Qiao, 2002; Qiao and Gao, 2007). Its total sediment thickness is about 9200 m in the Jixian section, which lies at the centre of the aulacogen. This failed rift may mark initial attempts at breakup of the Columbia supercontinent between 1600 and 1200 Ma (Rogers and Santosh, 2002; Qiao *et al*., 2007). Furthermore, many workers have proposed that this splitting event may have been responsible for the seismicity that generated much of the soft-sediment deformation in the region (Qiao, 2002; Qiao *et al*., 2007; Ettensohn *et al*., 2011). Subsequent folding and faulting in the Beijing area occurred during the Late Jurassic–Early Cretaceous Yanshanian Orogeny.

A systematic study of the geology of this area was initiated in 1934 (Kao *et al*., 1934). After many years of multidisciplinary study by numerous Chinese geologists, it is now generally accepted that the Meso-Neoproterozoic rocks of this area can be divided into 12 formations, which are (from the base upward), the Changzhougou, Chuanlinggou, Tuanshanzi, Dahongyu, Gaoyuzhuang, Yangzhuang, Wumishan, Hongshuizhuang, Tieling, Xiamaling, Longshan and Jingeryu formations (Fig. 2). The greatest part of the sequence is of Mesoproterozoic age, including the interval from the Changzhougou Formation to Xiamaling Formation. The Neoproterozoic rocks of the Longshan and Jingeryu formations are unconformably overlain by Cambrian limestones.

A large fault (>800 km long) runs from southwestern Shijiazhuang to northeastern Lingyuan and Tieling (Fig. 1B), along the axial part of the Yan-Liao Aulacogen. This Shijiazhuang–Lingyuan Fault was activated during the early Mesoproterozoic (He *et al*., 2000) and is regarded as the main trigger for ancient earthquakes (Qiao and Gao, 2007; Su and Sun, 2012). The first reported earthquake-triggered SSDS in China lies very close to this fault (Song, 1988; Site 1, near the Ming Tombs Area in Fig. 3). Since then, earthquake-triggered SSDS have been discovered in six more locations within the same general area indicated in Figure 1B (Site 2: Liu, 2001; Site 3: Liang *et al*., 2002; Sites 4 and 5: Qiao and Gao, 2007; Site 6: Liang *et al*., 2009; Ettensohn *et al*., 2011; site 7, this paper). Thus, it is generally believed that the SSDS in the Wumishan Formation are controlled or influenced by proximity to the Meso- to Neoproterozoic Shijiazhuang–Lingyuan Fault, as most sites exhibiting SSDS lie approximately less than 20 km from the fault.

The stratigraphic divisions and their sequence of formation are already well established. Historically, different schemes put forward by many geologists for the various formations have been incorporated and synthesized in 'The Regional Geology of Beijing Municipality' (Bureau of Geology and Mineral Resources of Beijing Municipality, 1991). However, the ages of these formations have been refined in the last few decades, because of new dating techniques. For example, the Wumishan Formation, the thickest and most widely distributed unit, had no isotopic age determinations prior to the 1980s. The first K–Ar isotopic dating of galena from the adjacent strata suggested ages between 1400 and 1220 Ma (Yu and Zhang, 1984). Several $^{40}Ar/^{39}Ar$ analyses obtained later from the chert nodule argued for an age of between 1310 and 1207 Ma for the Wumishan Formation (Wang *et al*., 1995). Since then, several SHRIMP U–Pb zircon ages have been published and their locations are marked in Figure 2 (Lu and Li, 1991; Gao *et al*., 2007, 2008; Li *et al*., 2010; Su *et al*., 2008; Su *et al*., 2010; He *et al*., 2011). Based on the newest and more precise dating, it is possible to constrain the age of the Wumishan Formation as between 1550 and 1450 Ma, i.e. lower Mesoproterozoic (Fig. 2; Bureau of Geology and Mineral Resources of Beijing Municipality, 1991).

DOI: 10.1002/gj

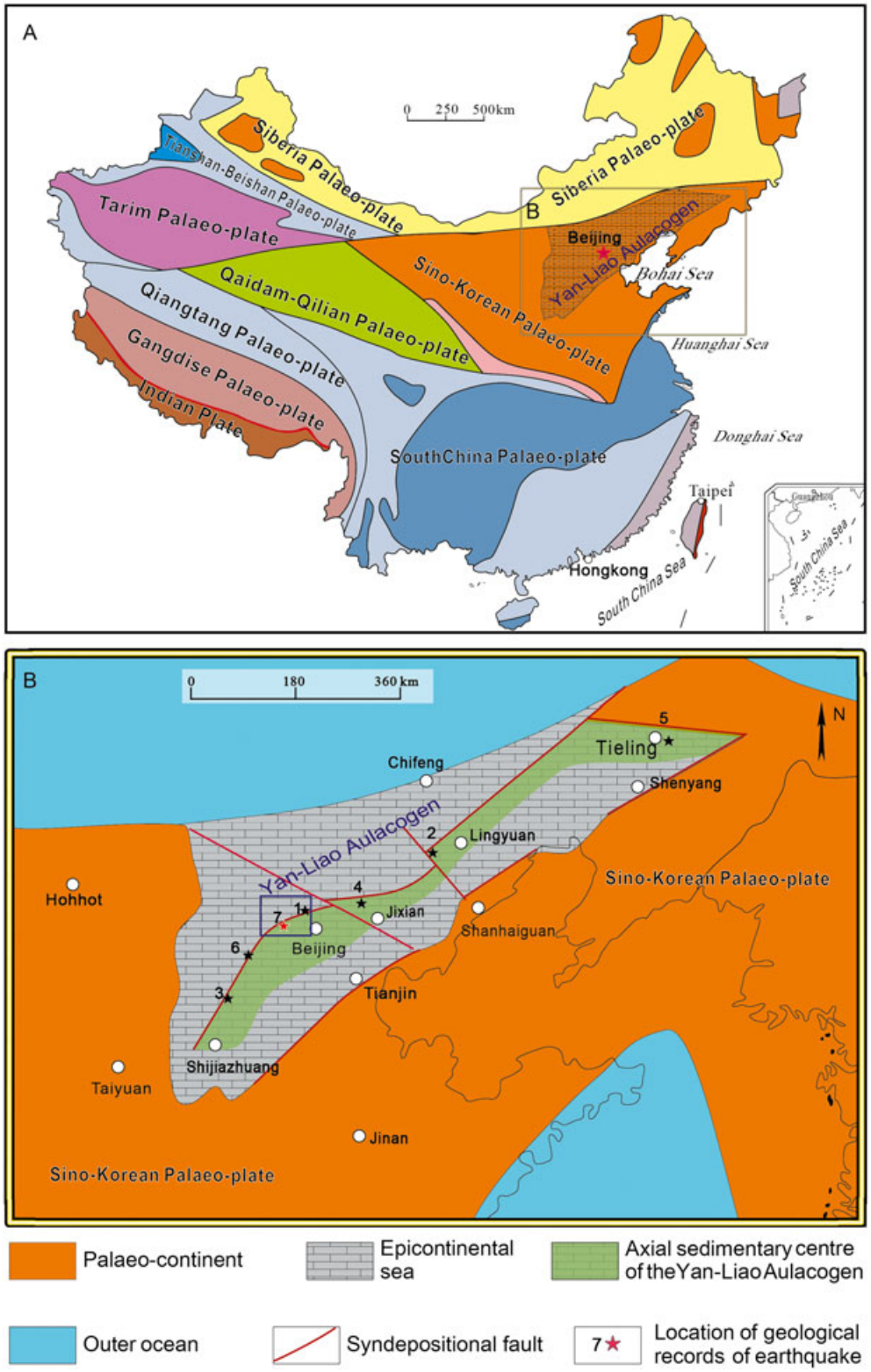

Figure 1. (A) Palaeo-plate map of China, showing the distribution of the major palaeo-plates of different ages (after Liu and Wang, 2007). (B) Palaeogeographical map of the Yan-Liao Aulacogen from the Proterozoic Gaoyuzhuang Stage to the Wumishan Stage, showing an epicontinental sea opened to the north (after He *et al*., 2000; Qiao, 2002; Qiao and Gao, 2007; Su and Sun, 2012). The locations of earthquake-triggered SSDS outcrops recorded by other geologists are shown as black stars (No. 1 to No. 6). The studied outcrop of the present contribution is marked by the red star (No. 7). The blue rectangle around the red star represents the study area. This figure is available in colour online at wileyonlinelibrary.com/journal/gj

DOI: 10.1002/gj

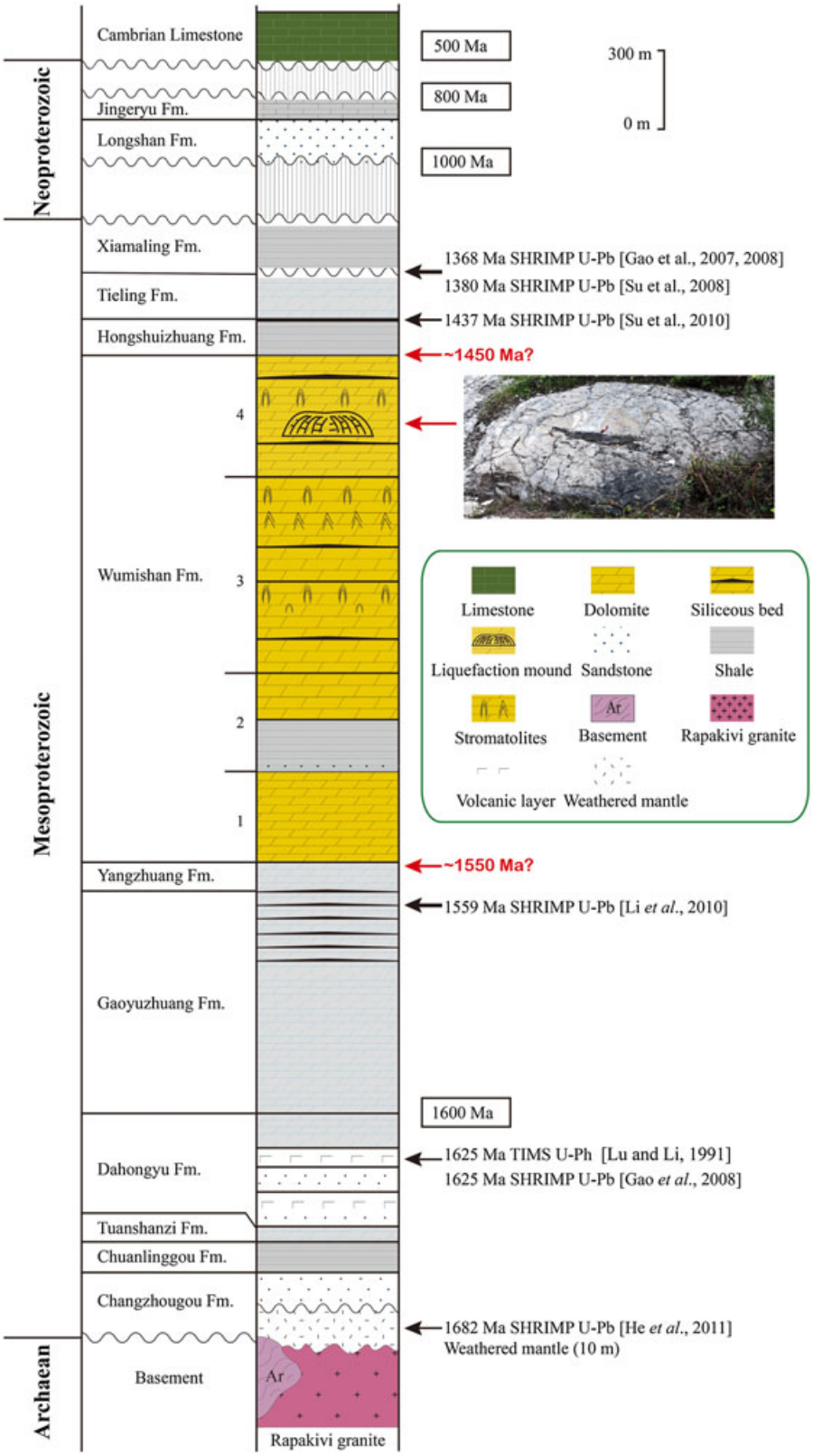

Figure 2. Lithostratigraphy of the Meso- and Neoproterozoic strata of the Yan-Liao Aulacogen and the approximate position of the newly discovered liquefaction mounds (Member 4, Wumishan Fm.). The newly published SHRIMP age data are shown on the right of the column. Based on these data, it is reasonable to deduce that the Wumishan Formation formed between 1550 and 1450 Ma. This figure is available in colour online at wileyonlinelibrary.com/journal/gj

DOI: 10.1002/gj

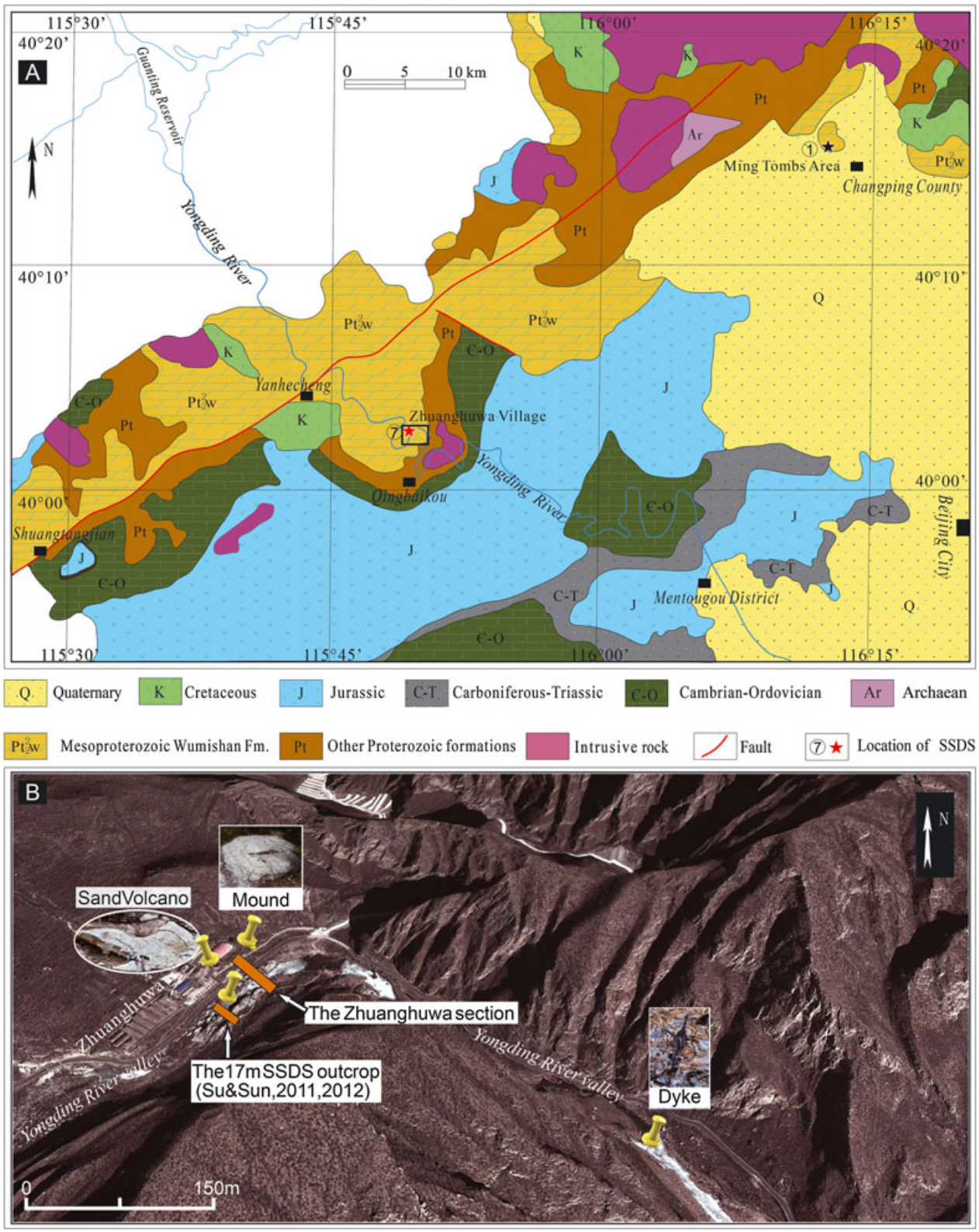

Figure 3. (A) Simplified geological map of the Yongding River valley area (see inset box in Fig. 1B for location), showing the distribution of the Mesoproterozoic Wumishan Formation, Zhuanghuwa village section (location 7) and the Ming Tombs Area (location 1) (After Su and Sun, 2012). (B) Satellite map of the Zhuanghuwa section, showing the relative positions of the section and some of the main liquefaction features. This figure is available in colour online at wileyonlinelibrary.com/journal/gj

DOI: 10.1002/gj

The Wumishan Formation crops out over about 12% of the Beijing area (*ca*. 2016 km^2; Fig. 3A). It consists mostly of well-laminated dolostones (*ca*. 89%) and silicified dolostones or siliceous chert rocks (10%). The remaining 1% of the rocks are thin shale interbeds and terrigenous sediments (sandstones). The total thickness of the Wumishan Formation is between 1500 m to 3495 m in the Beijing area. The Formation is largely composed of stacked peritidal parasequences, a few metres to tens of metres thick, separated by silty shales (Ettensohn *et al*., 2011). The parasequences show fining upward and shoaling upward. At the base are subtidal high-energy cross-bedded dolarenites. These pass up through lagoonal dolosiltites to low-energy peritidal laminites with mudcracks and stromatolites in the upper part of a parasequence. On the basis of the stacking patterns, the rock compositions, and the stromatolite characteristics, the Wumishan Formation is divided into four members (numbered 1–4 in Fig. 2). Member 1 is mainly composed of terrigenous sediments and bituminous dolostone. In the western area, a layer of quartz sandstone is usually developed in the basal part. In the local standard section in the Ming Tombs Area (Fig. 3), the thickness of Member 1 is about 450 m. The rock types of Member 2 vary sharply, from quartz sandstone to sandy dolostone, or laminated dolostone, reflecting the dramatic changes of the palaeo-environment. The thickness of Member 2 is about 400 m in the Ming Tombs Area. Member 3 is the thickest member in this formation (854 m in the Ming Tombs Area). The main rock types are laminated dolostone with abundant pillar/cone-shaped stromatolites. Member 4 is mainly composed of laminated thinly-bedded dolostone with banded cherty dolomite and occasional stromatolites. The discovery of the mounds is from this member (Member 4). Many well-preserved shallow-water sedimentary structures, such as ripple marks, cross-bedding and stromatolites, indicate that the Wumishan Formation accumulated, essentially, in a stable, shallow-water, peritidal platform environment (Fig. 4). These well-developed 'normal' sedimentary structures (especially the ripple marks and cross-bedding) also indicate that the dolomite from the Wumishan Formation has some features typical of shallow-water siliciclastic rocks. Sedimentary successions formed in such environments are, when still unlithified, highly susceptible to earthquakes, which may easily induce soft-sediment deformation structures (SSDS) in them, particularly within the laminites.

Numerous excellent outcrops of SSDS occur in the deeply incised and strongly scoured Yongding River valley, and the best outcrop is located near Zhuanghuwa Village (115°49′36″E longitude and 40°2′52″N latitude, Fig. 3). In a section only 17 m thick, nearly 30 layers containing earthquake-triggered SSDS have been identified (No. 7 location, the red star in Figs. 1 and 3; Su and Sun, 2011, 2012).

Ten liquefaction-induced mounds and one carbonate sand volcano were discovered on a privately owned property during fieldwork in August 2011. These occur at a horizon approximately 10 m below the above-mentioned outcrop. Subsequently, a typical carbonate dyke and several intrastratal faults were found in nearby outcrops. As will be documented below, these liquefaction-induced mounds, the sand volcano, and other SSDS structures provide direct evidence of earthquake activities at ~1500 Ma ago.

3. DISTRIBUTION AND DESCRIPTION OF THE MOUNDS AND THE CARBONATE SAND VOLCANO

Ten carbonate mounds and one crater-shaped sand volcano are recorded in the upper part of the Wumishan Formation, which is mostly composed of dolostone. Eight of the mounds crop out along a roadcut about 100 m long (115°49′36″E longitude and 40°2′52″N latitude); and the other two mounds were discovered about 10 m from the roadcut. All ten mounds occur in the same stratigraphic layer, where they have a generally rounded shape, with some concentric and radial fissures. The diameter of the mounds varies between 1.5 m to 4 m and their height from 10 cm to 30 cm (Fig. 5). All of the mounds are composed of grey dolostone with minor amount of black siliceous (chert) rock, especially on the top of the mounds. The main features of these mounds are summarized in Table 1.

The first and best exposed mound has an almost perfectly circular shape, with a diameter of 2.8 m. This mound is divided into six rings by concentric circular fissures, which are inclined about 40–60° into the centre (labelled from C1 to C6, core to margin, in Fig. 6A). There are 13 radial fissures emanating from the centre, which are mostly regularly spaced apart. The majority of the concentric and radial fissures are filled with dark siliceous chert rock. A shallow depression on the top of the mound is filled by 3–5 cm of siliceous rock, which is structureless and its composition is identical to that in the fractures.

The ninth structure in Figure 5 is half-covered by a stone wall (the top-left area of Fig. 7A). Its central upper part was also partly covered by soil when it was discovered. After being 'exhumed', it became obvious that this structure is shaped just like a small volcano with a crater (Fig. 7A). It has a diameter of 110 cm and the 'crater' at the top has a depth of about 30 cm. The thickness of the first layer of the 'crater' decreases dramatically, outwardly, from 30 cm in the highest point of the crater to 2 cm in the outer-edge, over a horizontal distance of only one metre. A thin layer of black siliceous rock is built up in the centre of the depression. There are also exposed at least three (possibly five) radial fractures which are filled with dark siliceous material (Fig. 7A). Between the top layer and the layer beneath, there is a thin layer of siliceous rock. Small samples were collected for thin-section petrography, as well as two larger slabs (Fig. 7B and 7C). The composition of the rock from

DOI: 10.1002/gj

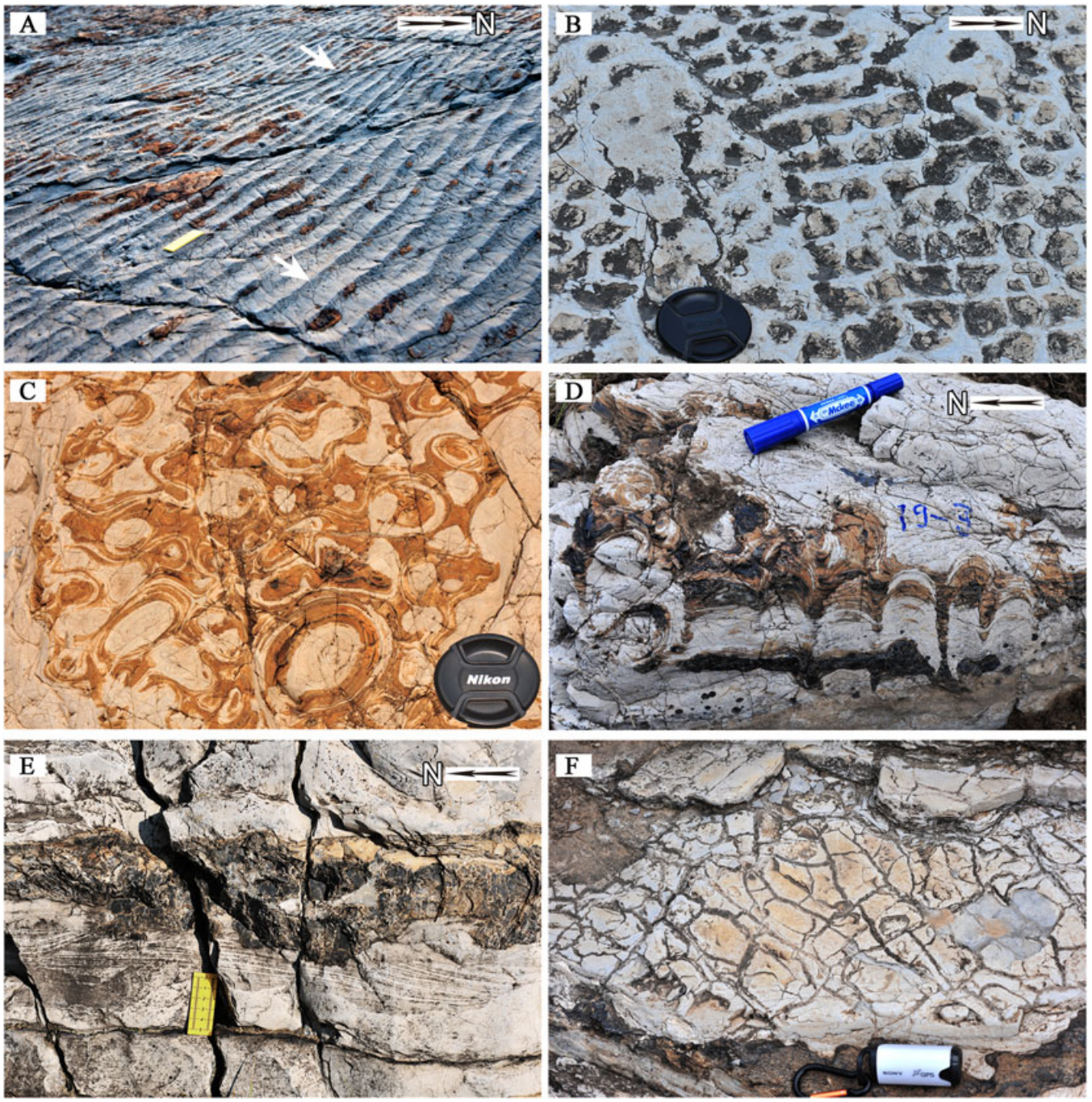

Figure 4. The assemblage of typical 'normal' sedimentary structures indicates a shallow-water depositional environment for the Wumishan Formation. (A) asymmetrical ripple marks on a bedding plane (The arrows represent the palaeocurrent direction –flow to the northwest); (B) interference ripples; (C) stromatolites in plan view on the top of this section; (D) Another layer of domal stromatolites, in profile, in the upper part of this section; (E) cross-lamination in dolarenite bed cut by a chert band; (F) mud cracks. (The yellow ruler in Fig. 4A is 10 cm long; the diameter of the lens cap in Fig. 4B and 4C is 8 cm; the blue marker pen is 14 cm long; the GPS tracker is 7.5 cm long). This figure is available in colour online at wileyonlinelibrary.com/journal/gj

Figure 7B is dolomicrite. The banding in Figure 7B is mainly the result of weathering. The deeper part of the sample has the darker colour. The irregular brecciated clasts at the top of the polished slab in Figure 7C are fractured dolomicrite, siliceous chert and secondary quartz sand grains (indicated by arrows). All the petrographic observations confirm the host rock is dolomicrite with a minor component of detrital quartz.

DOI: 10.1002/gj

Figure 5. Spatial distribution of eight liquefaction mounds (numbered 1 to 8) and one carbonate sand volcano (No. 9) along the road at the Zhuanghuwa section. The length of the hammer is 40 cm. View looking southwest. Beds dip gently to the east at 15–20°. Note that the margins of mounds 2 and 3 are indicated by a dotted line. This figure is available in colour online at wileyonlinelibrary.com/journal/gj

4. TYPICAL SOFT-SEDIMENT DEFORMATION STRUCTURES (SSDS) FROM YOUNGER STRATA ABOVE THE MOUNDS

Numerous SSDS features occur in the 17 m-thick outcrop section in the Yongding Valley and in several adjacent outcrops along the Yongding River. Most of these brittle and ductile structures, e.g. diapirs and clastic dykes, convolute bedding, accordion folds, plate-spine breccias and loop bedding have been already described before (cf. Su and Sun, 2011, 2012). Here, we only refer to new horizons of SSDS or features not documented previously in detail.

4.1. Clastic dykes

Usually, clastic intrusions (dykes and sills) in sediments develop when water and sediment (typically sand) flow from depth into fissures and along the base of an overlying fine-grained cap (Obermeier, 1996).

Two new layers with typical liquefaction-induced clastic dykes have been found less than 100 m stratigraphically above the layer containing the mounds and sand volcano in the Zhuanghuwa section.

As illustrated in Figure 8A, Layer II contains several dark coloured siliceous dykes (D1, D2 in Fig. 8A). D1 and D2 are morphologically not characteristic of liquefaction dykes, but the expansion of the bottom of the dykes and the dragging and bending of the surrounding sediments at the top, provide clear evidence that these pathways were involved in the formation of the overlying dark-coloured siliceous rocks.

The most typical liquefaction dyke occurs in layer III (d2 in Fig. 8A and 8B). This dyke is about 15 cm long and less than 1 cm thick. It is needle-like and its injection nature from below is very apparent. The surrounding rocks in Layer III-3 show clear deformation with dragging and bending upward of laminations at the upper end of the dyke. It was originally formed by disturbance and liquefaction of the water-saturated sediments from Layer III-2. Now the outer rim of the dyke has been silicified and become a halo of darker silica, but the middle part remains paler grey dolostone.

4.1.1. Interpretation

The dykes originally were the weak parts or cracks in the relatively unconsolidated dolostone layers when the liquefaction process started. Both the lithostatic overpressure from the overlying younger sediments and/or the pressure

DOI: 10.1002/gj

Table 1. Main features of the liquefaction mounds in Zhuanghuwa section, Yongding Valley

	Shape and dimensions	No. of concentric rings	No. of radial fractures	Silica at top surface	Depression at top surface
Mound 1	Circular; diameter is 2.8 m; height is 30 cm	6	13	Yes	Yes
Mound 2	Oval; longest axis is 3.3 m and the short axis 1.8 m; height is 20 cm	4	Not obvious	No	Yes
Mound 3	Circular. diameter is 3 m; height is 20 – 30 cm	2	>4	Yes	No
Mound 4	Circular. diameter is about 2.4 m; height is 20 cm	5	5	No	Yes
Mound 5	Circular. diameter is about 2.5 m; height is 15 cm	3	3	Yes	Yes
Mound 6	Irregular circular. The diameter varies from 3 to 4 m. height is 20 cm	7	7	Yes	Yes
Mound 7	Irregular circular. Partly covered by a wall. The longest axis is about 1.2 m; height is 10 cm	5	8	No	Yes
Mound 8	Circular. diameter is about 2 m; height is 15 cm	4-5	11	Yes	Yes

caused by seismic vibration can drive the underlying sediment to break through or be injected into the overlying layers and take the form of dykes. It is apparent that the siliceous material in layer II (Fig. 8A) and siliceous and carbonate material in layer III (Fig. 8B) was still comparatively unconsolidated when injected into the lithified carbonate beds (now dolostones). The well-developed columnar stromatolite features and other normal sedimentary structures in the Wumishan Formation showed that the cementation rate was very high and the compaction was limited. So the trigger for the formation of such injection dykes could hardly be the lithostatic overburden. Combined with the numerous SSDS structures (especially the widely believed seismic origin SSDS) found in this succession, we believe that these dykes were caused by vibration related to the earthquakes. This forced the dark unconsolidated (siliceous) sediment to penetrate into empty or weak areas in the light coloured dolostone to form clastic dykes with attendant deformation features, such as folding and bending in the laminated sediments (cf. Su and Sun, 2012).

4.2. *Fragmented breccias*

In the Zhuanghuwa section, two layers of *in situ* fragmented breccia are present. The first layer is about 10 m above the mound layer and is 10 cm thick. It is composed of mostly fragmented dolostone breccia, with angular fragments varying in size from several mm to up to 10 cm in size piled loosely together (Fig. 9A). The laminations in the fragments can be perfectly correlated. The second layer, also 10 cm thick, crops out about 5 m above the first breccia layer. It consists of a partly fragmented breccia, in which the fragments are closely packed together and the original features of the breccia layer (e.g. lamination and cross-lamination) could be recognized (Fig. 9B).

4.2.1. *Interpretation*

The first breccia layer suggests very little displacement of the clasts and is comparable to the autoclastic breccia of Montenat *et al*. (2007). In the second breccia layer sedimentary structures such as cross-stratification are present. Both breccia layers demonstrate deformation and fragmentation of brittle rocks. These breccia layers are interpreted by Su and Sun (2012) to have resulted from the shaking of the sediment during a large magnitude earthquake. Similar features have been described in fine-grained laminated silty and sand beds of the Orobic Basin, Southern Alps, which also exhibit injection dykes and possible sand volcanoes (Berra and Felletti, 2011). Their formation was suggested by these authors to indicate the effects of seismic shocks. Microbreccias similar to those in the Wumishan Formation have also been recorded in laminated microbialites in the Neuquén Basin, Argentina, associated with folds and faults and other earthquake-induced soft-sediment deformation structures (Martín-Chivelet *et al*., 2011).

4.3. *Compressional deformation structures*

Compressional SSDS are the most common seismic structures in the Wumishan Fm. in the study area. They include characteristic features, such as a special kind of accordion fold and the larger scale intrastratal folds.

The accordion fold is the most widely distributed syndepositional structure in the Wumishan Formation. It

DOI: 10.1002/gj

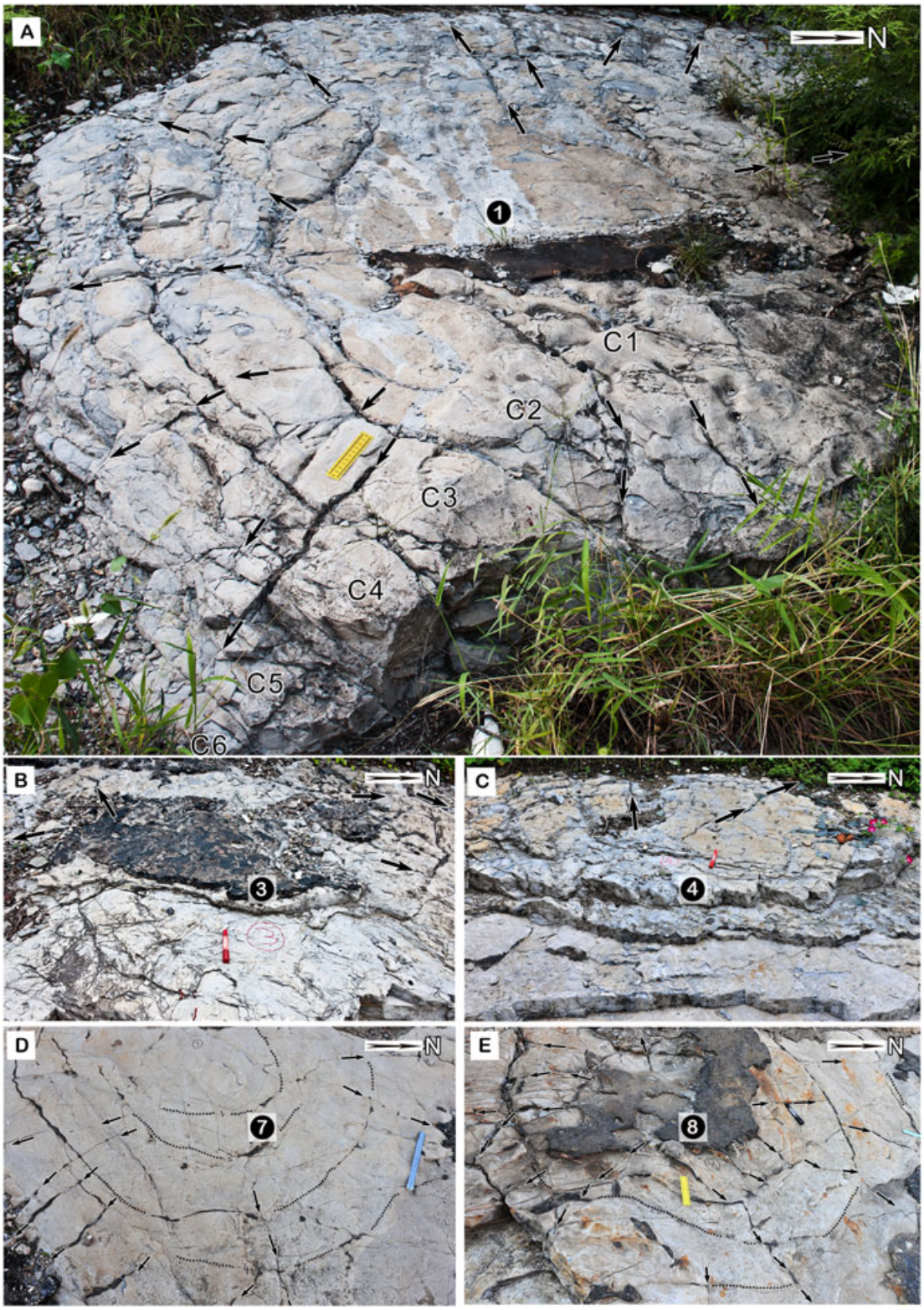

Figure 6. (A)–(E). Close-up views of five typical mounds from the Zhuanghuwa section illustrated in Figure 5. Figure 6A shows the best exposed and developed mound (mound 1). Note the concentric circular rings and the radial fissures (arrowed). The fourth and the eighth mounds (Fig. 6C, 6E) are also rounded, but the eighth is not topographically as high. The concentric rings in mounds 7 and 8 (Fig. 6D and 6E) are indicated by dotted lines and radial fractures by arrows. The numbers in the photos correspond to the mound numbers in Figure 5. The yellow ruler is 10 cm long. The red marker pen is 14 cm long. This figure is available in colour online at wileyonlinelibrary.com/journal/gj

DOI: 10.1002/gj

Figure 7. (A) The fine-grained carbonate-sand volcano at Zhuanghuwa section has a diameter of nearly 1.1 m. Note there are several radial fissures (arrowed), which have been filled by dark chert. (B)–(C). Two large polished samples at B and C (see 7A for location). There is no lamination present. The blue marker pen in 7A is 14 cm long. This figure is available in colour online at wileyonlinelibrary.com/journal/gj

DOI: 10.1002/gj

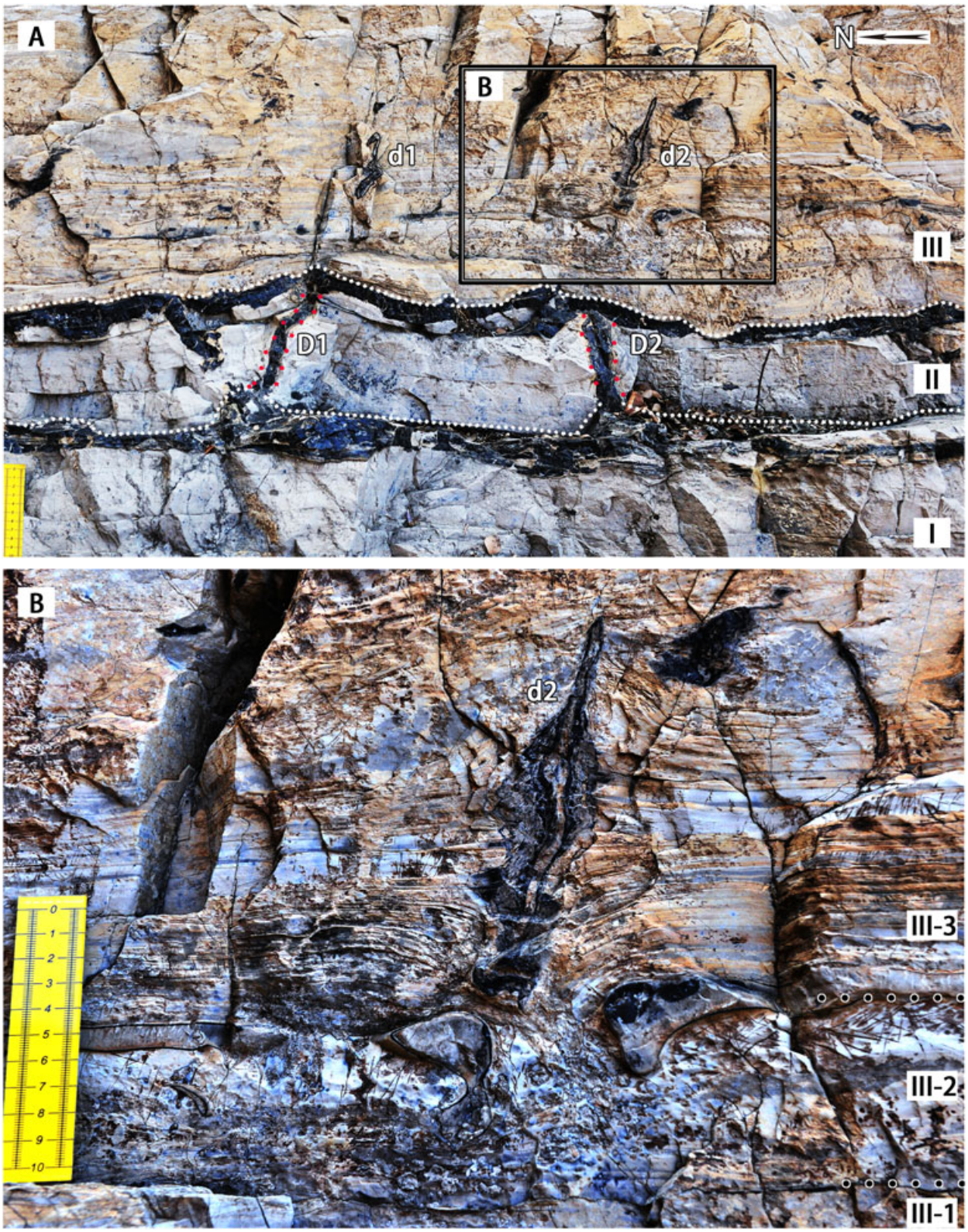

Figure 8. Liquefaction-induced dykes in bedded dolomite near the Zhuanghuwa section. (A) General view of the two layers (II and III) containing the siliceous and dolostone dykes. The dykes in Layer II (D1, D2) are much longer and wider than those in the lower part of Layer III (d1, d2). (B) Close-up of a typical dyke in Layer III. Note that the needle-like dyke is inclined slightly to the right (75°). Layer II is more siliceous and the colour is darker. This figure is available in colour online at wileyonlinelibrary.com/journal/gj

DOI: 10.1002/gj

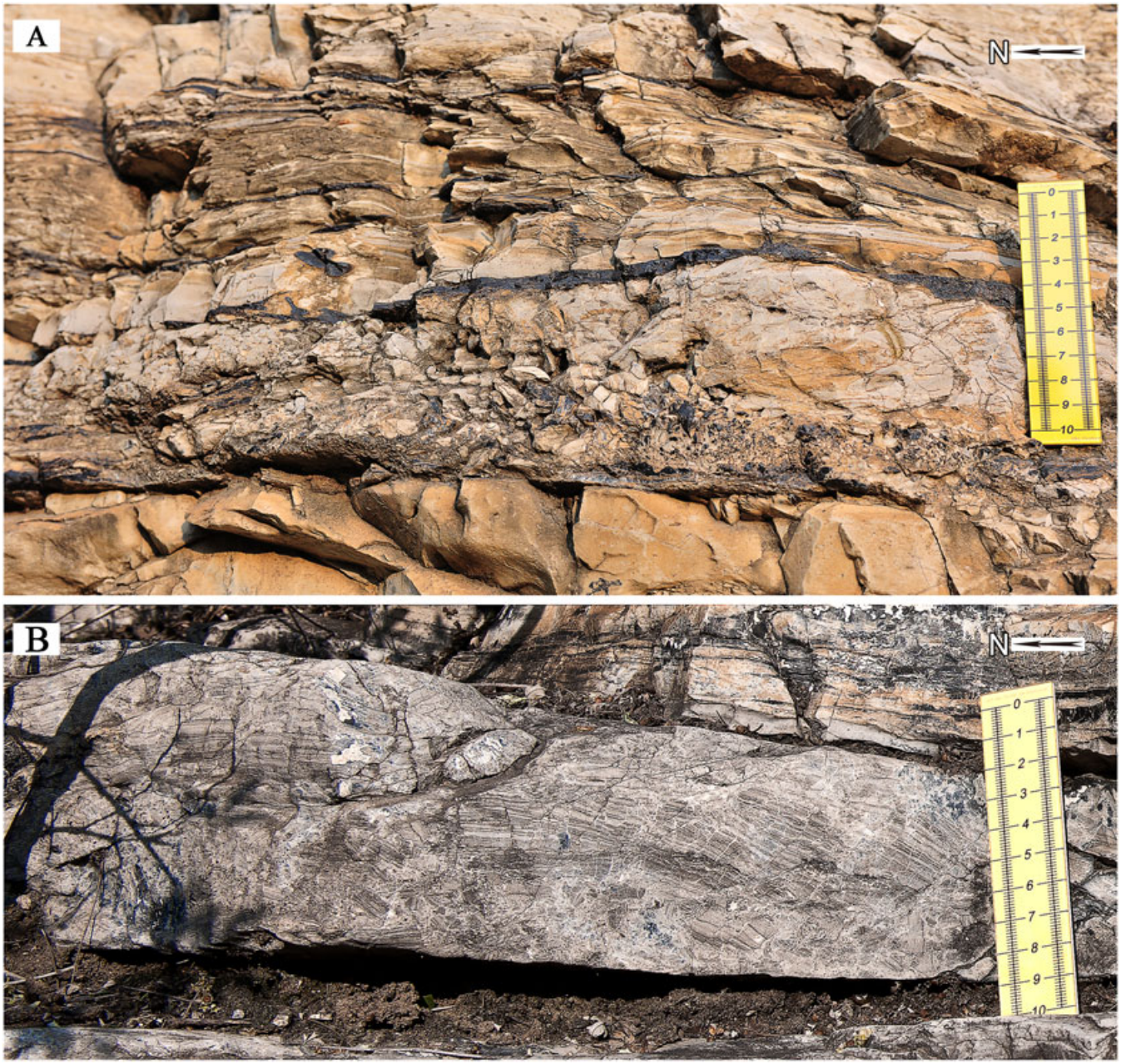

Figure 9. Two types of seismically fragmented breccia in the Zhuanghuwa section. (A) Completely fragmented breccia, with the fragments piled loosely together (in the lower part of the outcrop in the valley); (B) Partly cracked *in situ* breccia, with all breccia fragments being closely packed (in the middle part of the section). This figure is available in colour online at wileyonlinelibrary.com/journal/gj

has been regarded as an important indicator of seismic activity by many geologists (Song, 1988; Song and Einsele, 1996; Qiao and Li, 2009; Ettensohn *et al*., 2011). A systematic description and analysis of the genetic processes of different kinds of accordion folds in the study area were given by Su and Sun (2011, 2012). Here we just discuss the larger scale intrastratal folds.

Two layers show strong intrastratal folds. The first layer occurs in the upper part of the Zhuanghuwa section, and is about 20 cm thick. The mud cracks and ripple marks beneath this layer indicate a very shallow-water depositional environment. There are no signs of any deformation either in the layer above or in the layer beneath (Fig. 10A).

The second is the strongest folded layer in this section, occurring just several metres above the carbonate mound layer. The whole layer comprising several thinly-bedded laminated units is about 30 cm thick and is strongly folded (Fig. 10B). The adjacent layers are unfolded.

DOI: 10.1002/gj

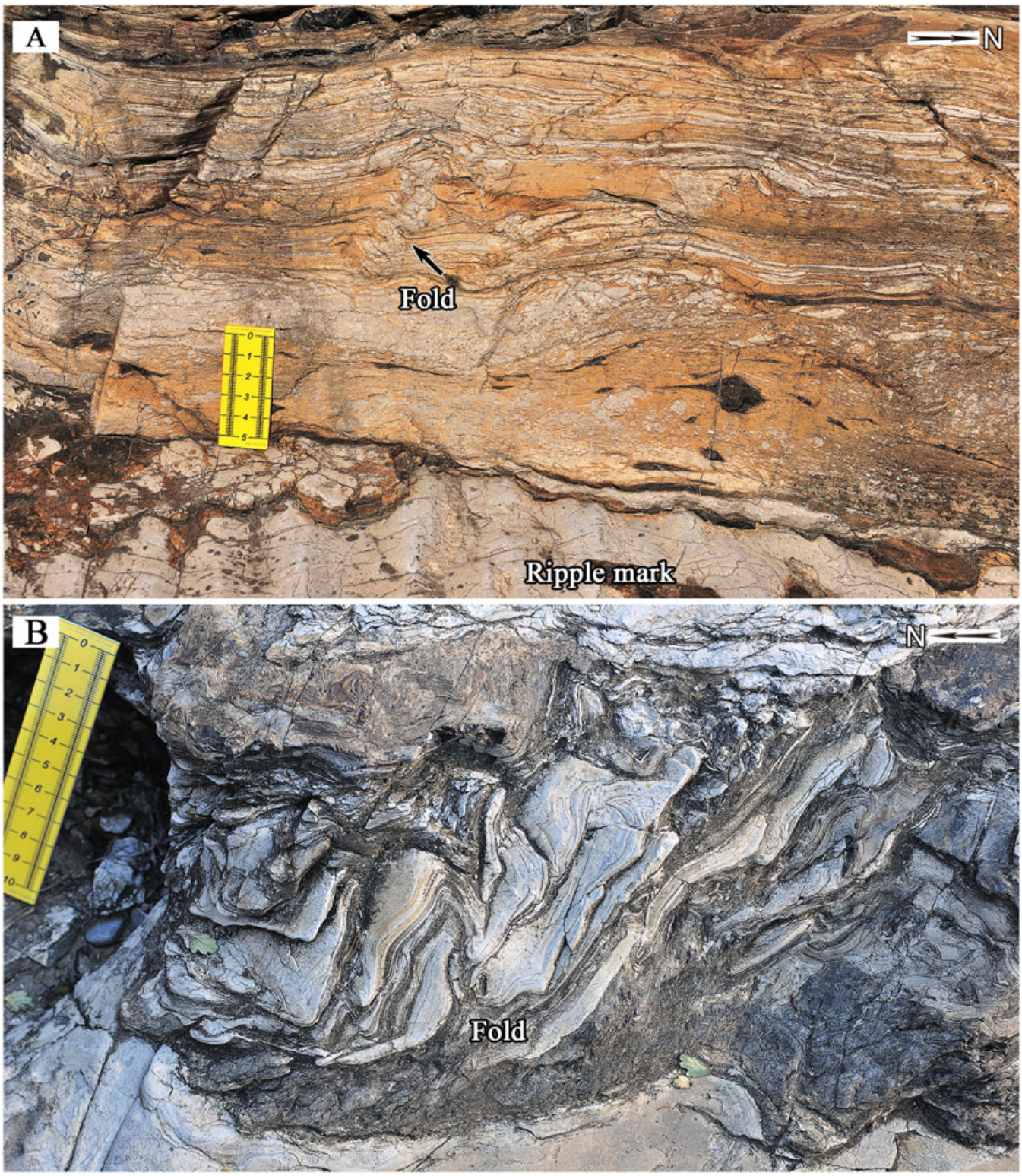

Figure 10. Layers with compressional intrastratal folds. (A) Layer with intrastratal folding in the upper part of the section. Note that the folds are concentrated in the middle part of the layer (arrowed). The shallow-water ripple marks occur just beneath this layer. (B) Layer with intrastratal enterolithic folding in the lower part of the section. The entire layer is folded, indicating stronger compressional stress. Note the underlying and overlying beds are unfolded. Scale: ruler is 5 cm long in A; 10 cm long in B. This figure is available in colour online at wileyonlinelibrary.com/journal/gj

DOI: 10.1002/gj

4.3.1. Interpretation

The two folded layers are possibly related to separate ancient seismic events. In fact, the second folded layer is the same as the intrastratal deformation strata recorded by Ettensohn *et al*. (2011, fig. 14) and explained as the possible product of seismogenic activity. If other conditions (such as cementation and composition) were the same, the strengths of the earthquakes should be different. The absence of any fold structure in the enclosing strata demonstrates that these seismites are confined to discrete stratigraphic horizons.

Figure 11. Intrastratal thrust faults in the Zhuanghuwa section. (A) The fault occurs in a single dolomite layer without extending into adjacent strata. The repeated chert band demonstrates the compressional nature of the fault. The age of this kind of fault is basically the same as that of the surrounding rock. The yellow ruler is 10 cm long. (B) Two faults cut through Layer 17-1 but do not extend into the overlying Layer 17-2 or the underlying Layer 16, indicating that they formed later than Layer 17-1, but earlier than Layer 17-2. Note also the difference in orientation of faults F1 and F2/F3 in Figure 11A and 11B respectively. A is about 50 m stratigraphically higher than B in the field. The blue marker pen is 14 cm long. This figure is available in colour online at wileyonlinelibrary.com/journal/gj

DOI: 10.1002/gj

4.4. *Intrastratal faults*

Several layers containing intrastratal thrust faults occur in the Zhuanghuwa section. Most of the faults are simple and short, often restricted to one single layer. They usually are less than 100 cm long and 'die out' at both ends as a result of 'absorption' of the stress by the surrounding material (Fig. 11A).

There is another kind of intrastratal fault, which cuts through the whole layer but does not extend into the overlying or underlying strata. Typical examples were found in the middle part of the Zhuanghuwa section, where two microthrust-faults occurred in one layer (F2 and F3 in Fig. 11B).

4.4.1. *Interpretation*

The fault planes are usually relatively low angle, indicating that the thrust faults were formed at an early diagenetic stage, as seen by the repetition of chert bands (Fig. 11A). The microthrusts in Figure 11B, confined to a single bed, indicate that there was a time lag between the accumulation of the sediment and the faulting (Fig. 11B). Interstratal low-angle reverse (thrust) faults have been recorded in the laminated carbonates of the Neuquén Basin associated with other SSDS structures (Martín-Chivelet *et al*., 2011), such as microbreccias and asymmetric folds, attributed to large earthquakes.

4.5. *Summary*

The range of injection structures – diapirs and dykes of both carbonate and siliceous material, and breccias – argues for the dominance of liquefaction-related deformation in the Wumishan Formation. Moreover, those deformations are regarded by Ettensohn *et al*. (2011) as the highest level of liquefaction-related deformation, and hence they conclude are related to a seismogenic cause. The abundance of relatively small-scale intrastratal phenomena such as accordion folds reflects the well-bedded and thinly-bedded laminated nature of the upper Member 4 of the Wumishan Formation. In addition, as much of the sedimentary facies is peritidal, early lithification would have been predominant and would have facilitated brittle fracture and liquefaction or fluidization processes (see Zhang *et al*., 2007; Ettensohn *et al*., 2011; Su and Sun, 2012). Studies by Jolly and Lonergan (2002) suggest that common liquefaction structures such as clastic intrusions form from earthquakes with a magnitude of 5.5–6 as the lower limit. Furthermore, higher magnitude earthquakes (>6) are required to produce seismically-induced soft-sediment deformation at a distance of 15–20 km from the epicentre (Sims, 1975; Hempton and Dewey, 1983; Mohindra and Bagati, 1996; Blanc *et al*., 1998; Galli, 2000).

5. DISCUSSION

5.1. *The genetic mechanism of the mounds*

There are two main possible genetic mechanisms for the development of the mounds in the Wumishan Formation. The first is by biogenic processes. The second is by liquefaction/fluidization of soft carbonate sediments, especially the earthquake-triggered liquefaction/fluidization mechanism.

The genesis of the mounds as a biological structure, such as a stromatolite can be excluded for the following reasons. (1) There are numerous stromatolitic biogenic structures in the Wumishan Formation, but all of them are dome-shaped, without any signs of a depression in the top-central part (Fig. 6C and 6D). (2) There are obvious laminations in the stromatolites in both the outer part and the inner part of the mound structure. No signs of any cyanobacterial-induced laminated structures have been observed either macroscopically, from the external morphology or microscopically from the inner structure of these mounds. (3) Thin-section studies from the mound reveal the obvious liquefaction

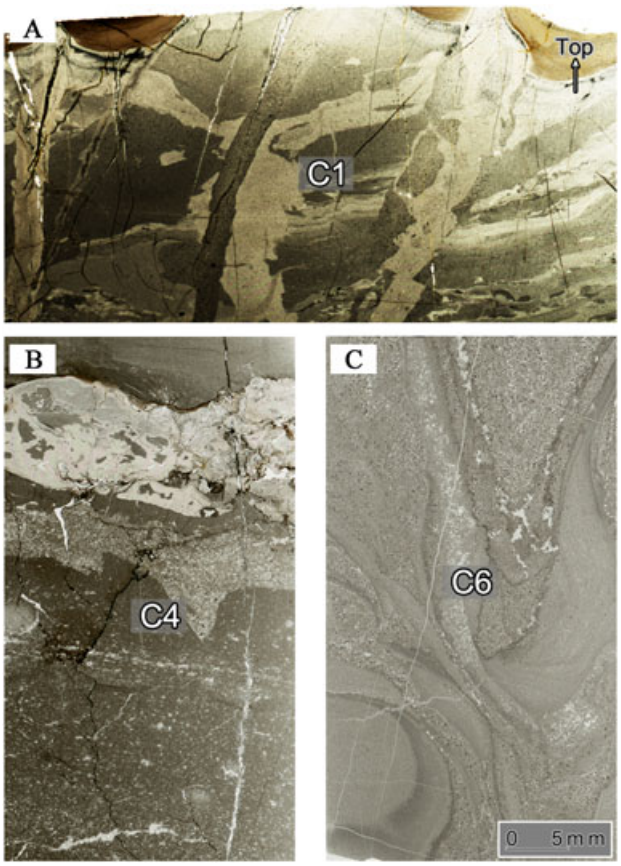

Figure 12. (A)–(C). Thin-section photos of the first mound. C1, C4 and C6 are the same rings as those indicated in Figure 6. A is from the centre of the mound (C1) and showed interpenetration of the lighter part into the darker part. B showed some features of breccias in ring 4 (C4). C is from the outer part of the mound (C6) and showed obvious features of fluidification. This figure is available in colour online at wileyonlinelibrary.com/journal/gj

DOI: 10.1002/gj

disturbance and signs of fracturing in the inner part of the mound (Fig. 12). Thus, the mechanism for the genesis of the mounds must therefore be related to liquefaction/fluidization.

Experiments on the fluidization of layered sediments and the formation of water-escape and gas-escape structures have been conducted in the laboratory by several researchers (e.g. Nichols *et al*., 1994; Owen, 1996; Moretti *et al*., 1999). The experiments of Nichols *et al*. (1994) demonstrated that fluid-escape structures can be formed once the balance of the overlying material and the base layer was disturbed by unstable fluidization behaviour. Their experiments showed clearly the development of fluid-escape structures. Normally, the sand volcano is the final product, while the mound-shaped structure is the intermediate product of their experiments. The results of their experiments are very consistent with our actual field observations.

Early lithification of carbonate is another likely reason for the forming and preserving of the mound.

5.2. The trigger of the liquefaction mounds and the sand volcano

It is well known that many agencies may trigger the liquefaction of sediments. To investigate the real triggers for liquefaction-induced SSDS, we need to consider as many aspects as possible about the formation process of (liquefaction) SSDS and to understand the overall sedimentological and palaeo-environmental settings.

The following features need to be highlighted:

(1) The possible influence of gases produced by organic matter on these structures could be excluded because there is insufficient organic matter on the Earth during the Mesoproterozoic.
(2) Based on the sedimentological, palaeogeographical and structural data mentioned above, and already published, the Wumishan Formation was deposited in a tectonically active aulacogen (Song and Einsele, 1996; Wen, 1997; He *et al*., 2000; Qiao, 2002; Qiao and Gao, 2007; Song and Liu, 2009). Previous studies have found seismites in six different sites along the large axial fault of the aulacogen (Fig. 1). This fault was active during the early Mesoproterozoic and has been regarded as the main trigger for ancient earthquakes (Liu, 2001; Liang *et al*., 2002; Qiao and Gao, 2007; Liang *et al*., 2009; Ettensohn *et al*., 2011).
(3) There is already one special SSDS feature which is widely distributed in the Wumishan Formation. It was originally called the 'spine-plate' breccia by most Chinese geologists and was subsequently renamed the

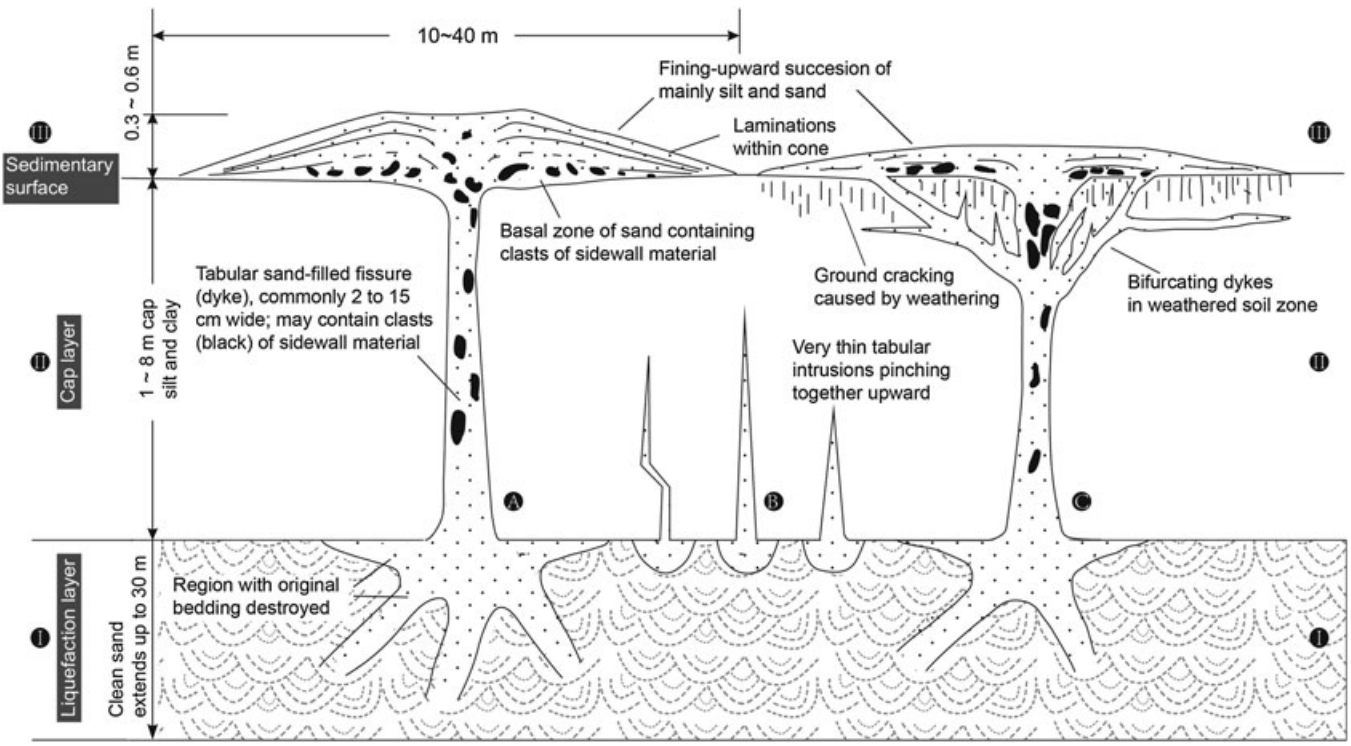

Figure 13. Schematic vertical section showing idealized dykes cutting through silt and clay strata. Sketches are based mainly on field observations of the 1811–1812 New Madrid (Missouri) earthquakes, from the Wabash Valley of Indiana–Illinois, and from islands in the lower Columbia River of Oregon–Washington. All dykes are tabular in planar view whether they vent to the surface or pinch together. (A) Stratigraphy of a dyke with sediment vented to the surface. (B) Dykes that taper as they ascend. (C) Dyke characteristics often associated with a fractured zone of weathering that develops in high-plasticity clays (modified from Obermeier, 1996).

DOI: 10.1002/gj

'accordion fold' by Ettensohn *et al.* (2011). The accordion fold has been regarded as an important indicator of seismic activity by many geologists (Song, 1988; Song and Einsele, 1996; Qiao and Li, 2009; Ettensohn *et al.*, 2011).

(4) Nearly all the phenomena associated with the mounds, such as carbonate/siliceous clastic dykes, syndepositional faults and folds, and fragmented breccias documented herein, could be explained by proximity to the large active synsedimentary Shijiazhuang–Lingyuan Fault. Moreover, most of the deformational phenomena are restricted to discrete horizons in the Wumishan Formation and are interstratal.

In fact, liquefaction-induced mounds, sand volcanoes and clastic dykes are common liquefaction features in modern-day areas affected by strong earthquakes (Obermeier, 1996, 1998; Takahama *et al.*, 2000). Many researchers have noticed the close relationship between the fluidization/liquefaction structures (especially the sand volcanoes) and the vibrations of the earthquakes (Bonini, 2009; Manga *et al.*, 2009; van Loon and Maulik, 2011). The unconsolidated and water-saturated sediments can liquefy by the strong vibrations caused by an earthquake. The vibrations may cause the pore-water pressure to multiply within seconds. This pressure can hydraulically fracture an overlying fine-grained sediment cap and lead to the upward escape of large quantities of sediment and water to the surface, resulting in the formation of sand mounds or sand volcanoes (Obermeier, 1996, 1998; Takahama *et al.*, 2000; Manga *et al.*, 2009). Obermeier (1996) has developed an idealized genetic model for the liquefaction-induced dykes, based on many years of exploration and study of liquefaction features in the USA, especially field observations of the 1811–1812 New Madrid earthquakes in Missouri (Fig. 13).

(5) Many similar liquefaction mounds were formed due to the 2008 Wenchuan Earthquake (Ms 8.0) in West Sichuan Province, southwest China. This earthquake is related to the Longmen Shan Fault system that marks the boundary

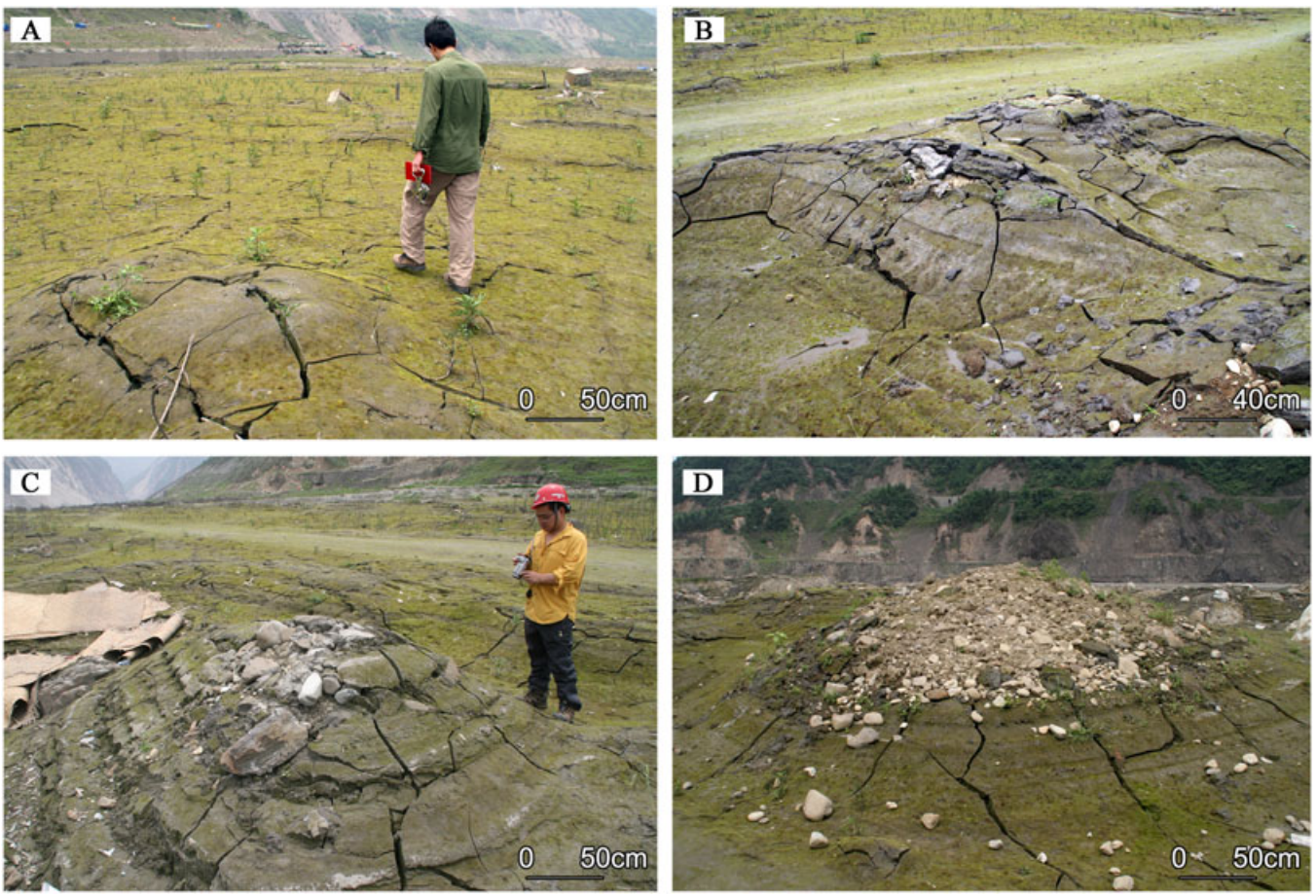

Figure 14. Liquefaction-induced mounds formed by the Wenchuan Earthquake in 2008, showing the various stages of development (after Qiao and Li, 2009). This figure is available in colour online at wileyonlinelibrary.com/journal/gj

DOI: 10.1002/gj

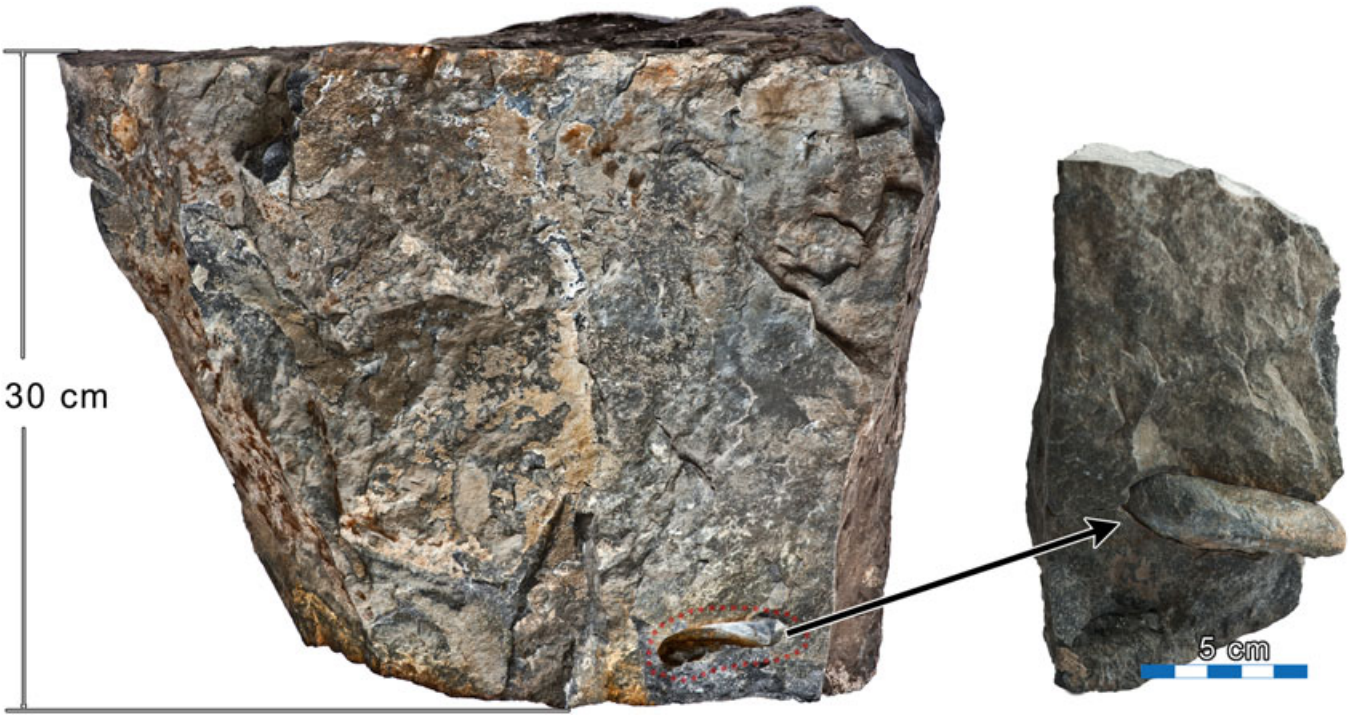

Figure 15. A characteristic gravel particle from the bottom and centre part of the mound. The surrounding dolomite is about 30 cm thick, whereas the gravel particle is 7 cm long and 4 cm wide. This figure is available in colour online at wileyonlinelibrary.com/journal/gj

between the Precambrian Pengguan Massif (Eastern Tibet Plateau) and the Mesozoic sediments of the Sichuan Basin (Royden *et al*., 2008). The fault system has a history of mostly right-lateral strike–slip but also thrust motion (Densmore *et al*., 2007).

Four representative examples of the mounds are illustrated in Figure 14 (Qiao and Li, 2009). They also represent the four developmental stages of seismic liquefaction-induced mounds. Figure 14A shows the product of the initial stage of the liquefaction. The land surface was pushed upwards by the liquefied sand, so that a mound-like feature was formed with radial cracks. Ongoing liquefaction led to more liquefied sand being vented to the sedimentary surface by the pore-water pressure; the mound thus became higher and larger, but hardly any sand flowed out at the surface during this stage. At the same time, the radial cracks continued to grow centrifugally, step by step, and concentric fissures were produced (Fig. 14B). When the pore-water pressure became large enough, the liquefied sand and even some gravel reached the sedimentary surface, starting to flow out (Fig. 14C). As more sand and gravel flowed out at the surface, a mound was eventually formed (Fig. 14D). The composition of the liquefaction-induced mound is two-fold: part of the outer crust and bottom consists of the *in situ* sand and soil, whereas the main part consists of the sand and gravel that originally formed part of the liquefied sand layer deeper down. These two parts are commonly mixed up and are then called 'chaotic sediments' (Takahama *et al*., 2000).This is exactly what happened in the area that was affected by the Wenchuan Earthquake. The morphological similarity between the carbonate mounds in the Mesoproterozoic Wumishan Fm. and the mounds associated with recent earthquakes is very clear. We can see clearly the gravels erupted to the surface.

(6) To testify the genetic model of Obermeier (1996), we broke one corner of the biggest mound (the No. 1 mound). Some 20–70 mm gravel-sized dolostone particles were found at the bottom part of the mound when some pieces were cut off from the mound (Fig. 15).

This example indicates that the genetic process of the Mesoproterozoic mounds and related liquefaction products in a carbonate environment is similar to that of the clastic sedimentary environment. Overmeier's 1996 genetic model can also be used to explain the Mesoproterozoic liquefaction-induced dykes, the mounds and the sand volcano in the study area.

Based on the above reasons, we believe that the most likely trigger for the formation of the liquefaction mounds and volcano is ancient earthquake shaking.

6. CONCLUSIONS

Liquefaction-induced mounds and sand volcanoes are rarely preserved in the geological record. The liquefied sand is

DOI: 10.1002/gj

vented to the surface only during, or directly after, the earthquake-induced vibrations. Normally, once the vibrations stop, some of the liquefied sand will be sucked back into the original space. Only parts of the chaotic sediments thus are left (Takahama *et al*., 2000). As for the material that flowed out at the surface, this forms mounds and sand volcanoes, which have a positive form (topographic high) on the sedimentary surface. These positive forms are consequently exposed to erosion and/or abrasion due to the activity of bottom currents and/or waves (van Loon and Maulik, 2011).

Some of the earliest known sand volcanoes date from the Upper Carboniferous of western Ireland (Gill and Kuenen, 1958) and Early Permian in eastern India (van Loon and Maulik, 2011). Liquefaction-induced mounds had thus far been reported only in the Holocene Period. Thus, the liquefaction-induced mounds and the carbonate sand volcano in the Mesoproterozoic Wumishan Formation are the earliest examples of these features, with an age of nearly 1500 Ma.

The trigger mechanism of the liquefaction for the forming of these mounds, the carbonate sand volcano and other related SSDS in well-laminated carbonate are similar to those in clastic rocks. These features can all be regarded as the result of Mesoproterozoic earthquake activity associated with the Shijiazhuang–Lingyan Fault. The frequency and intensity of seismic activity during the Mesoproterozoic Wumishan stage should be very strong. The mechanism of generating high magnitude earthquakes at that time was basically the same as nowadays, with attendant features produced.

ACKNOWLEDGEMENTS

The authors are deeply indebted to Prof. Paul Robinson and Prof. Tom van Loon for their instructive comments and scientific remarks. We owe our gratitude to the two anonymous reviewers for their helpful comments and suggestions. The authors dedicate their contribution for this article to the newly opened State Key Laboratory of Continental Structures and Dynamics, of the Chinese Academy of Geological Sciences in recognition of the support and assistance of all members of the Laboratory.

REFERENCES

Bachmann, G.H., **Aref, M.A.M. 2005**. A seismite in Triassic gypsum deposits (Grabfeld Formation, Ladinian), southwestern Germany. *Sedimentary Geology* **180**, 75–89.

Berra, F., **Felletti, F. 2011**. Syndepositional tectonics recorded by soft-sediment deformation and liquefaction structures (continental Lower Permian sediments, Southern Alps, Northern Italy): Stratigraphic significance. *Sedimentary Geology* **235**, 249–263.

Blanc, E.J.-P., **Blanc-Alétru, M.-C.**, **Mojon, P.-O. 1998**. Soft-sediment deformations structures interpreted as seismites in the uppermost Aptian to lowermost Albian transgressive deposits of the Chihuahua Basin (Mexico). *Geologisches Rundschau* **86**, 875–883.

Bonini, M. 2009. Mud volcano eruptions and earthquakes in the Northern Apennines and Sicily, Italy. *Tectonophysics* **474**, 723–735.

Bureau of Geology and Mineral Resources of Beijing Municipality. 1991. *Regional Geology of Beijing Municipality*. Geological Publishing House: Beijing, 68–81 (In Chinese, with English Abstract).

Densmore, A.L., **Ellis, M.A.**, **Li, Y.**, **Zhou, R.**, **Hancock, G.S.**, **Richardson, N. 2007**. Active tectonics of the Beichuan and Pengguan faults at the eastern margin of the Tibetan Plateau. *Tectonics* **26**, TC4005. DOI: 10.1029/2006TC001987.

Ettensohn, F.R., **Zhang, C.H.**, **Gao, L.Z.**, **Lierman, R.T. 2011**. Soft-sediment deformation in epicontinental carbonates as evidence of paleoseismicity with evidence for a possible new seismogenic indicator: Accordion folds. *Sedimentary Geology* **235**, 222–233.

Galli, P. 2000. New empirical relationships between magnitude and distance for liquefaction. *Tectonophyiscs* **324**, 169–187.

Gao, L.Z., **Zhang, C.H.**, **Shi, X.Y.**, **Zhou, H.R.**, **Wang, Z.Q.**, **Song, B. 2007**. A new SHRIMP age of the Xiamaling Formation in the North China Plate and its geological significance. *Acta Geologica Sinica* **81**, 1103–1109.

Gao, L.Z., **Zhang, C.H.**, **Yin, C.Y.**, **Shi, X.Y.**, **Wang, Z.Q.**, **Liu, Y.M.**, **Liu, P.J.**, **Tang, F.**, **Song, B. 2008**. SHRIMP zircon ages: Basis for refining the chronostratigraphic classification of the Meso- and Neoproterozoic strata in North China Old Land. *Acta Geoscientica Sinica* **29**, 366–376 (In Chinese, with English Abstract).

Gill, W.D., **Kuenen, P.H. 1958**. Sand volcanoes on slump deposits in the Carboniferous of County Clare, Ireland. *Quarterly Journal of the Geological Society of London* **133**, 441–460.

He, Z.J., **Song, T.R.**, **Ding, X.Z.**, **Zhang, Q.**, **Meng, X.H.**, **Ge, M. 2000**. Early synsedimentary faulting of the Meso-Proterozoic Yanshan rift and its influence on event sedimentation. *Journal of Palaeogeography* **2**, 83–91 (In Chinese, with English Abstract).

He, Z.J., **Zhang, X.Y.**, **Niu, B.G.**, **Liu, R.Y.**, **Zhao, L. 2011**. The paleoweathering mantle of the Proterozoic rapakivi granite in Miyun County, Beijing and the relationship with the Changzhougou Formation of Changchengian System. *Earth Science Frontiers* **18**, 123–130 (In Chinese, with English Abstract).

Hempton, M.R., **Dewey, J.S. 1983**. Eathquake-induced deformational structures in young lacustrine sediments. East Anatolian Fault, southeast Turkey. *Tectonophysics* **98**, 7–14.

Jolly, R.J.H., **Lonergan, L. 2002**. Mechanism and controls on the formation of sand intrusions. *Journal of the Geological Society of London* **159**, 605–617.

Kao, C.S., **Hsiug, Y.H.**, **Kao, P. 1934**. Preliminary notes on Sinian stratigraphy of North China. *Bulletin of Geological Society of China* **13**, 243–288.

Li, H.K., **Zhu, S.X.**, **Xiang, Z.Q.**, **Su, W.B.**, **Lu, S.N.**, **Zhou, H.Y.**, **Geng, J.Z.**, **Li, S.**, **Yang, F.J. 2010**. Zircon U–Pb dating on tuff bed from Gaoyuzhuang Formation in Yanqing, Beijing: Further constraints on the new subdivision of the Mesoproterozoic stratigraphy in the North China Craton. *Acta Petrologica Sinica* **26**, 2131–2140.

Liang, D.Y., **Song, Z.M.**, **Zhao, C.H.**, **Nie, Z.T. 2002**. Discovery of Mesoproterozoic seismites at Baishi Mountain, Hebei Province and its geological significance. *Geological Bulletin of China* **21**, 625–630.

Liang, D.Y., **Nie, Z.T.**, **Song, Z.M.**, **Zhao, C.H.**, **Chen, K.G.**, **Gong, H.B. 2009**. Seismic-tsunami sequence and its geological features of Mesoproterozoic Wumishan Formation in Fangshan Global Geopark, Beijing, China: a case study on Yesanpo scenic district. *Geological Bulletin of China* **28**, 30–37 (In Chinese, with English Abstract).

Liu, P.J. 2001. Seismite and its rhythm in the Gaoyuzhuang Formation of Mesoproterozoic in Pingquan County, Hebei Province. *Geoscience* **15**, 266–269 (In Chinese, with English Abstract).

Liu, X.Y., **Wang, Q. 2007**. Plate tectonic map of China's lithosphere. In: *Geological Atlas of China*, Ma, L.F., Qiao, X.F., Min, L.R., Fan, B.X., Ding, X.Z. (eds). Geological Publishing House: China, 41–44 (in Chinese).

van Loon, A.J. 2009. Soft-sediment deformational structures in siliciclastic sediments: An overview. *Geologos* **15**(1), 3–55.

van Loon, A.J., **Maulik, P. 2011**. Abraded sand volcanoes as a tool for recognizing paleo-earthquakes, with examples from the Cisuralian

Talchir Formation near Angul (Orissa, eastern India). *Sedimentary Geology* **238**, 145–155

Lu, S.N., **Li, H.M. 1991**. A precise U–Pb single zircon age determination for the volcanics of the Dahongyu Formation, Changcheng System in Jixian. *Chinese Academy of Geological Science Bulletin* **22**, 137–146 (In Chinese, with English Abstract).

Manga, M., **Brumm, M.**, **Rudolph, M. 2009**. Earthquake triggering of mud volcanoes. *Marine and Petroleum Geology* **26**, 1785–1798.

Martín-Chivelet, J., **Palma, R.M.**, **López-Gómez, J.**, **Kietzmann, D.A. 2011**. Earthquake-induced soft-sediment deformation structures in Upper Jurassic open-marine microbialites (Neuquén Basin, Argentina). *Sedimentary Geology* **235**, 210–221.

Mohindra, R., **Bagati, T.N. 1996**. Seismically induced soft-sediment structures (seismites) around Sumdo in the lower Spiti valley (Tethys Himalaya). *Sedimentary Geology* **101**, 69–83.

Montenat, C., **Barrier, P.**, **Ott d'Estevou, P.**, **Hibsch, C. 2007**. Seismites: An attempt at critical analysis and classification. *Sedimentary Geology* **196**, 5–30.

Moretti, M., **Alfaro, P.**, **Caselles, O.**, **Canas, J.A. 1999**. Modelling seismites with a digital shaking table. *Tectonophysics* **304**, 369–383.

Nichols, R.J., **Sparks, R.S.J.**, **Wilson, C.J.N. 1994**. Experimental studies of the fluidization of layered sediments and the formation of fluid escape structures. *Sedimentology* **41**, 233–253.

Obermeier, S.F. 1996. Use of liquefaction-induced features for paleoseismic analysis – an overview of how seismic liquefaction features can be distinguished from other features and how their regional distribution and properties of source sediment can be used to infer the location and strength of Holocene paleo-earthquakes. *Engineering Geology* **44**, 1–76.

Obermeier, S.F. 1998. Liquefaction evidence for strong earthquakes of Holocene and latest Pleistocene ages in the states of Indiana and Illinois, USA. *Engineering Geology* **50**, 227–254.

Owen, G. 1987. Deformation processes in unconsolidated sands. In: *Deformation of Sediments and Sedimentary Rocks*, Jones, M.E., Preston, R.M. F. (eds), Geological Society, London, Special Publication **29**, 11–24.

Owen, G. 1996. Experimental soft-sediment deformation: structures formed by liquefaction of unconsolidated sands and some ancient examples. *Sedimentology* **43**, 279–294.

Qiao, X.F. 2002. Intraplate seismic belt and basin framework of Sino-Korean plate in the Proterozoic. *Earth Science Frontiers* **9**, 141–150 (In Chinese, with English Abstract).

Qiao, X.F., **Gao, L.Z. 2007**. Mesoproterozoic palaeoearthquake and palaeogeography in Yan-Liao Aulacogen. *Journal of Palaeogeography* **9**, 337–352 (In Chinese, with English Abstract).

Qiao, X.F., Li, H.B.. 2009. Effect of earthquake and ancient seismites on sediments. *Journal of Palaeogeography* **11**, 593–610 (In Chinese, with English Abstract).

Qiao, X.F., **Gao, L.Z.**, **Peng, Y. 2007**. Mesoproterozoic earthquake events and breakup of the Sino-Korean Plate. *Acta Geologica Sinica (English Edition)* **81**, 385–397.

Rogers, J.J.W., **Santosh, M. 2002**. Configuration of Columbia, a Mesoproterozoic supercontinent. *Gondwana Research* **5**, 5–22.

Rossetti, D.F., **Góes, A.M. 2000**. Deciphering the sedimentological imprint of paleoseismic events: An example from the Aptian Codo´ Formation, northern Brazil. *Sedimentary Geology* **135**, 137–156.

Royden, L.H., **Burchfiel, B.C.**, **van der Hilst, R.D. 2008**. The geological evolution of the Tibetan Plateau. *Science* **321**(5892), 1054–1058.

Sims, J.D. 1975. Determining earthquake recurrence intervals from deformational structures in young lacustrine sediments. *Tectonophysics* **29**, 141–152.

Song, T.R. 1988. A probable earthquake-tsunami sequence in Precambrian carbonate strata of Ming Tombs District, Beijing. *Chinese Science Bulletin* **33**, 1121–1124.

Song, T.R., **Einsele, G. 1996**. Proterozoic sedimentary facies and their depositional environments in the Ming Tombs District, Beijing. In: *Field trip Guide T201 of the 30th International Geological Congress*. Geological Publishing House: Beijing, T201.1–T201.22.

Song, T.R., **Liu, Y.X. 2009**. Ancient Earthquake Records and Litho-Palaeogeography. *Acta Sedimentologica Sinica* **27**, 872–879.

Su, D.C., **Sun, A.P. 2011**. Soft-sediment deformation and occurrence frequency of palaeoearthquake in the Mesoproterozoic Wumishan Formation, Yongding River Valley, Beijing. *Journal of Palaeogeography (Chinese Edition)* **13**, 591–614 (In Chinese, with English Abstract).

Su, D.C., **Sun, A.P. 2012**. Typical earthquake-induced soft-sediment deformation structures in the Mesoproterozoic Wumishan Fm., Yongding River valley (China) and interpreted earthquake frequency. *Journal of Palaeogeography (English Edition)* **1**, 71–89.

Su, W.B., **Zhang, S.H.**, **Huff, W.D.**, **Li, H.K.**, **Ettensohn, F.R.**, **Chen, X. Y.**, **Yang, H.M.**, **Han, Y.G.**, **Song, B.**, **Santosh, M. 2008**. SHRIMP U–Pb ages of K-bentonite beds in the Xiamaling Formation: Implications for revised subdivision of the Meso- to Neoproterozoic history of the North China Craton. *Gondwana Research* **14**, 543–553.

Su, W.B., **Li, H.K.**, **Huff, W.D.**, **Ettensohn, F.R.**, **Zhang, S.H.**, **Zhou, H.Y.**, **Wan, Y.S. 2010**. SHRIMP U–Pb dating for a K-bentonite bed in the Tieling Formation, North China. *Chinese Science Bulletin* **55**, 3312–3323.

Takahama, N., **Otsuka, T.**, **Brahmantyo, B. 2000**. A new phenomenon in ancient liquefaction – The draw-in process, its final stage. *Sedimentary Geology* **135**, 157–165.

Wang, S.S., **Sang, H.Q.**, **Qiu, J.**, **Chen, M.**, **Li, M.R. 1995**. The forming ages of Yangzhuang and Wumishan Formations in the Jixian section, Northern China. *Scientia Geologica Sinica* **30**, 166–173 (In Chinese, with English Abstract).

Wen, X. 1997. The failed rift model and stratigraphic division of Middle–Upper Proterozoic strata in the northern part of North China. *Progress in Precambrian Research* (In Chinese) **20**, 21–28.

Youd, T.L. 1973. Liquefaction, flow, and associated ground failure. *US Geological Survey Circular* **688**, 1–12.

Yu, R.B., **Zhang, X.Q. 1984**. Isotopic Geochronology Research on the Late Cambrian in Yanshan Area. *Bulletin of the Geology and Mineral Resources of Tianjin* **11**, 1–23 (In Chinese).

Zhang, C., **Wu, Z.**, **Gao, L.**, **Wang, W.**, **Tian, Y.**, **Ma, C. 2007**. Earthquake-induced soft-sediment deformation structures in the Mesoproterozoic Wumishan Formation, North China, and their geologic implications. *Science in China (Series D)* **50**, 350–358.

Scientific editing by Rob Hillier

DOI: 10.1002/gj